Development and Application of a Flexible and Efficient Environment for Aerodynamic Shape Optimisation

J. Brezillon, O. Brodersen, R. Dwight, A. Ronzheimer, J. Wild
German Aerospace Center (DLR)
Lilienthalplatz, 7 ,
D-38108 Braunschweig
Germany

Abstract

Within the next few years, numerical shape optimization based on high fidelity methods is likely to play a strategic role in future aircraft design. In this context, suitable tools have to be developed for solving aerodynamic shape optimisation problems. Based on the unstructured RANS solver *TAU*, the major key components recently developed, like for instance the free form deformation or the adjoint approach, are described in detail and applied for optimising the DLR-F6 wing-body aircraft configuration. Such application has permitted to assess the flexibility and the efficiency of the mesh procedure, the optimisation strategy, the adjoint approach and the parametrisation.

Key words: Optimisation; Adjoint; Aerodynamic; Aircraft; Wing Design

1. Introduction

Numerical shape optimisation based on high-fidelity methods will play a strategic role in future aircraft design. It offers the possibility of designing or improving aircraft components with respect to a given objective, subject to geometrical and physical constraints. Consequently, worldwide a large effort is being devoted to developing efficient optimisation strategies for industrial aerodynamic aircraft design.

For several years, activities at the DLR have focused on developing several key technologies important for the establishment of an efficient and flexible numerical optimisation capability based on high fidelity methods [18,19,20,21]. These include suitable techniques for geometry parametrisation, meshing and mesh movement methods, efficiency and accuracy improvements of the flow solvers used as well as robust and efficient optimisers.

The aim of the paper is to give an overview of the latest work on the development of a flexible and efficient optimisation chain and its application for the aerodynamic redesign of a 3d wing-body configuration. One key component of the aerodynamic chain is the unstructured finite-volume RANS solver DLR-*TAU* code. The wing parametrisation and the mesh procedure used to generate unstructured meshes will be described in detail. This aerodynamic chain is coupled to two types of optimisers: gradient free and gradient based optimisers. For the latter, the required gradients are efficiently computed due to the discrete adjoint formulation recently extended for 3d cases in the DLR-*TAU* code.

As an application, the geometry of the DLR F6 wing-body configuration is redesigned at a transonic flow condition with the objective of minimizing the drag at a given lift coefficient.

2. Test Case Definition

The flexibility to reuse the developed optimisation chain on other design problems and the efficiency to solve a given design problem are assessed on a simple but realistic aerodynamic problem and for this purpose the DLR F6 wing body configuration has been selected (see Fig. 1). The DLR-F6 configuration which was designed 20 years ago faces the difficulty that flow separations occur on the wing upper side at the junction of wing and fuselage and at the trailing edge ranging from about 30% up to 90% wing span.

The design concerns the complete wing and therefore the wing-fuselage intersection line has to be recomputed accordingly. In order to be close to a realistic design and to demonstrate the flexibility of the chain, the geometry is expressed in CAD form during the whole optimisation process. It is important to recall that the goal of the study is to assess the flexibility and efficiency of the optimisation chain. For this reason, we voluntarily limit the design to a total drag decrease at a given lift, transonic Mach number and Reynolds number; C_L=0.5, M_∞=0.75 and Re=3x10^6 respectively. The latter is representative of the model tested in the ONERA S2 wind-tunnel.

3. Unstructured RANS Solver TAU

One major key component for building flexible and efficient optimisation environment based on high fidelity

tools is the *TAU* software. It is a finite volume vertex-based solver with an edge-based data structure. Together with a dual-grid technique, CFD computations are possible on various mesh types [14,15]. Time integration to steady state is accomplished either using the backward Euler LUSGS or the Runge-Kutta scheme. An improvement of the convergence rate and the turn around time is achieved with multigrid and message-passing-interface (MPI)-based parallelisation [35].

For the optimisations, the *TAU* code is running in viscous mode. The Reynolds averaged Navier-Stokes equations are discretised using a central differencing scheme and a Jameson-type scalar dissipation. The turbulence is modelled with the one-equation Spalart-Allmaras with Edwards modifications [12,29]. The *TAU*-code is running in target-lift mode in order to compute the aerodynamic state at a given lift coefficient by automatically adjusting the angle of incidence.

The advantage of the adjoint method is its ability to evaluate the gradient of a single cost function with respect to a large number of design variables with an effort that scales weakly with the number of design variables [16,23]. For this reason, a discrete adjoint of the Navier-Stokes equations has been first developed in the *TAU*-code for two dimensional flows [9]. The method consists of the explicit construction of the exact Jacobian of the spatial discretisation with respect to the unknown variables allowing the adjoint equations to be formulated and solved. A wide range of the spatial discretisations available in *TAU* have been differentiated, including the Spalart-Allmaras-Edwards one-equation turbulence model. The effect of various approximations of the Jacobian was first investigated and the efficiency of this approach has been demonstrated on several 2d optimisation problems [1,10]. The formulation has recently been extended to 3d cases [11]. In the present study, some difficulties have been encountered regarding the convergence of the 3d adjoint equations. To overcome this problem, the turbulent effects are frozen during the adjoint computation. The metric terms required for the gradient computation are reliably evaluated by finite differences which imply the necessity of deforming the mesh in response to each shape-modifying design variable.
This process can be done during the CFD run and once the aerodynamic and adjoint states are available, the gradient is extremely fast to compute.

4. Geometry Representation and Parametrisation

For optimisation based on high fidelity tools, geometrical fidelity is of major importance and the geometry generation process represents the link between design parameters, which are driven by the optimiser, and simulation, which generally starts with the generation of corresponding meshes for CFD analyses.

In the context of our development, the complete wing has to be parametrised, which implies an update of the wing-fuselage intersection line for each deformation. Therefore a parameterisation purely based on wing mesh points could not be used and a CAD like representation is preferred. Secondly, the parametrisation has to be flexible enough to be applied later on other part of the aircraft like the nacelle. Regarding these constraints, the freeform deformation technique is an appropriate candidate and has already been applied for wing or belly-fairing optimisations at the DLR [25,26].

Freeform deformation (FFD) can be outlined as a mapping and re-mapping of object points into tri-variante B-Spline volumes, which are defined by their control point lattices, as shown in Fig. 2. During the mapping step parametric coordinates are calculated from given Cartesian coordinates via a Newton iteration method. A variation of the object is now achieved indirectly by the movement of certain control points of the corresponding lattice before the re-mapping is carried out. Furthermore, as far as the order of the B-Spline volumes is greater than 3, the continuity in curvature of the object shape is preserved. Therefore, the primary use of FFD is seen in aerodynamic shape optimisation, where curvature plays an important role.

The previously described freeform deformation algorithm has been implemented into the DLR mesh generation system MegaCads, which provides a broad palette of functionalities for CAD and structured mesh generation [4]. MegaCads is also well suited for the construction of proper control point lattices. The general procedure is now to split the geometry into parts and to construct adequate control point lattices around those parts which are designated for optimisation [25]. After the deformation of each part, the new intersection lines are recomputed and the final geometry is passed to the mesh generator. All individual parametric construction steps are recorded in a replay file, which is later replayed in every optimisation step.

As an application, 24 control points are used for the lattice around the F6 wing and to keep the wing planform unchanged, the points at the corners are not allowed to change. The vertical coordinate of the 8 red points in Fig. 2 are then directly used as design variables.

5. Meshing Procedures

In the present study, two different types of meshing procedures are investigated. The first one is based on hybrid meshes using prismatic elements for the resolution of the boundary layer. The second one is a mixture of structured/unstructured meshes meaning that hexahedral elements are used for the boundary layer resolution.

5.1. Hybrid Mesh Generation

The hybrid meshes, consisting of prismatic, pyramidal, and tetrahedral elements, have been generated with the Centaur® software package from CentaurSoft

[17] [7]. The software has an interactive part for the preparation of the CAD model, the specification of the boundary conditions, e.g. viscous wall and far field, and for the definition of element sizes. The data of the initial setup is used by the second part of the software package for the automatic, non-interactive generation of a hybrid mesh. In addition a tool is available to update the initial setup with a new geometry while maintaining the boundary conditions and sizing options so that a fully automatic mesh generation becomes possible which is necessary for the optimisation loop. However, this procedure does not guarantee an identical point discretisation of the geometry resulting in changing discretisation errors during the design process.

The mesh density and quality have a significant influence on the flow solution for the initial DLR-F6 configuration due to the flow separations. Two AIAA "Drag Prediction Workshops" held in 2003 and 2006 have shown that results for DLR-F6 drag computation vary significantly for different meshes whereas delta drag values can be computed with a good reliability [5,22]. This has been shown for several F6 configurations [6].

The mesh for the F6 wing-fuselage configurations has 24,335 points on the wing surface, 4,899 points on the fuselage surface, and 20 layers of prismatic elements. In total the mesh consists of 867,266 points (see Fig. 3). The complete setup of the initial hybrid mesh including trials of different mesh resolutions takes about 1 or 2 days.

5.2. Mixed Structured/Unstructured Mesh Procedure

The shortcoming of purely hybrid meshes is the low anisotropy of surface triangles resulting in a large number of surface mesh points, especially in spanwise direction for wings with high aspect ratios. On the other hand, the introduction of high anisotropy surface triangles would lead to too big discretisation errors in the CFD solution. With the application of structured meshes, the aspect ratios of surface quadrilaterals can be orders of magnitude higher, without loss of accuracy. However, the increasing complexity of the configuration to be meshed limits the application of purely structured meshes mainly because of the intricate mesh topology needed.

In the mixed mesh approach, simple block structured meshes with highly stretched hexahedral cells are employed for the boundary layer and the outer flow field is meshed using tetrahedral elements. The connection between both domains is accomplished by egg-carton like pyramids. It has already been shown that applying this mesh technique can greatly speed up Navier-Stokes flow computations without losing solution accuracy, mainly due the reduced number of points [33]. A further step towards flexibility has recently been achieved by developing an automatic generator for prismatic layers with triangular cross-sections, helpful in mesh regions of complex topology [34].

The mixed structured / unstructured mesh generation procedure described above has been implemented in MegaCads. For the generation of the unstructured mesh part the 3d triangulation software NETGEN of Schöberl was incorporated in MegaCads as a Black-Box tool [28]. The pyramidal elements connecting the structured with the unstructured mesh part are extruded from the hexahedral elements based on edge lengths in order to achieve a smooth transition of the control volumes for the reduction of numerical errors and instabilities.

Following this procedure, a first fine mesh for the F6 wing-fuselage configurations has been generated with 15,956 points on the wing surface, 13,870 points on the fuselage surface, and 25 layers of hexahedral elements. This mesh is presented in Fig. 3. In total the mesh consists of 728,763 points where 94% are located in the structured part. This construction of the initial mixed mesh with MegaCads requires more experience than using CentaurSoft and approximately 1 to 2 weeks of work is demanded. However, thanks to the parametric script technique of MegaCads, other meshes with the same topology can be generated automatically. For the purpose of the paper, a coarse mesh was designed in order to conduct several optimisations in a short turn around time. This second mesh only has 118,911 points.

For the computation of the gradients using the adjoint solution, an identical discretisation of the geometry is required. To insure this during the optimisation process, the structured part around the geometry is generated each time using MegaCads and an advancing front algorithm, available in the *TAU* code, deforms the unstructured part. This mesh procedure is called mixed mesh process and for comparison purposes is used for all optimisations involving mixed structured/unstructured meshes.

5.3. Verification on the Baseline Mesh

The main difficulty in designing a mesh for optimisation is to find the best compromise between accuracy and CPU time. Indeed, in a design process where hundred of computations are required, a very fine mesh would give an accurate solution but at a too large turn around time.

The first step before starting any optimisation is then to check that the main flow characteristics are captured in an acceptable turn around time. Figure 4 shows the pressure distribution at 2 sections, one close to the kink and the other close to the wing tip, measured in wind tunnel experiment and computed with the hybrid and mixed meshes. All data are obtained at the aerodynamic condition as described in Section 2. The agreement between computations and experiment is relatively good, and the fine mixed mesh is able to correctly predict the shock strength and position, mainly in the first part of the wing (close to the fuselage). In contrast, close to the wing tip, differences occur and these can be attributed to the structural effects which occur during the wind tunnel and are not taken into account in the numerical simulation.

In addition the computed flow separations on the wing upper side of the F6 are different for the hybrid and

the mixed meshes. Using the hybrid mesh the wing-fuselage and the trailing edge separations are significantly underestimated compared to the solution on the mixed mesh (see Fig. 5). Similar influences of the mesh on the flow solutions for F6 have already been observed by various authors in two AIAA Drag Prediction Workshops and will be not addressed here [8,22].

It can be pointed out that the pressure distributions for the coarse mixed mesh show a reduced pressure peak and shock strength but the main flow features, e.g. flow separations, are captured as plotted in Fig. 5.

Regarding the CPU time, a converged solution with change less than 0.01 counts in lift and drag is obtained after 5,000 iterations for all meshes. A CFD computation on 16 processors of a SUN AMD Opteron cluster takes 133 and 30 minutes on the fine and coarse mixed meshes respectively, and 158 minutes on the hybrid mesh.

The purpose of the study is not to perform a single accurate redesign of the wing-body configuration but rather to check the flexibility and efficiency of different strategies. It was therefore decided to mainly perform optimisation on the hybrid and mixed coarse meshes. For comparison purposes, the aerodynamic drag improvement obtained with the coarse mixed mesh process is checked afterwards on the finest mixed mesh.

6. Optimisation Strategies

6.1. Optimiser

Optimisation techniques for numerical problems are very well-explored and several hundred algorithms exist, which makes it difficult to test them all for 3d design. Furthermore, a pure non-deterministic approach, like genetic algorithms, requires too much CFD computations to converge and we voluntary limit our investigation to two kinds of deterministic strategies: a gradient free approach (simplex) and a gradient based strategy.

The simplex method is a deterministic gradient free strategy, so called because it uses neither random number nor derivatives [24]. One possible extension of this approach is the subplex method which first determines an appropriate set of subspaces and then uses the simplex to find a minimum in each subspace [27]. This permits one to treat bigger design problem without loss of convergence rate. The treatment of constrained optimisation problems can easily be handled by applying penalties on the objective function. Generally, this approach is particularly robust and performs well when the sensitivities differ considerably between design variables. It was successfully used at the DLR to carry out various high-lift optimisations [3,31,32].

Other deterministic approaches to minimise the objective function use the derivatives as a "search direction". The optimum is then sought following this searching direction and this process is repeated until derivatives are vanished or no improvement is obtained. The convergence rate of the design process can be drastically improved by simply taken the conjugate direction [30]. The latter was successfully used on various airfoil optimisations and tends to be more robust than more sophisticated approaches like quasi Newton trust region, when inaccurate gradients are used [10]. Several ways to handle constrained problems exist and good experience with the modified method of feasible direction has been achieved at the DLR [2,30]. The gradient based approaches are well known to converge extremely fast, as long as the derivatives are accurately computed. For this reason, the derivatives are evaluated here using either central finite differences or the adjoint approach.

6.2. Optimisation Frameworks

Modularity and flexibility of an aerodynamic optimisation framework is of main interest. Indeed it controls the optimisation loop which consists of the setting of the optimisation variables, the geometry modelling and mesh generation, as well as converting and scaling of the mesh, calling the *TAU* RANS solver and calculating the objective function for the optimiser.

In the present study, two types of framework have been used: the first one, internally developed at DLR, is based on a shell script techniques and the second one is commercial software.

During the design of the shell script based framework, it has been taken into account that the geometry modelling and the mesh generation run in a sequential mode whereas the flow solution can be performed in parallel on a high performance cluster. In addition the process can be distributed to different machines or can run completely on a parallel cluster taking a queuing system into account.

Regarding the commercial framework, the SynapsPointer® Pro (SPP) optimisation framework has been used because it allows an easy definition of the aerodynamic chain and connection to various machines [13]. Furthermore, a specific interface has been designed for the use of the adjoint approach and has been successfully used in the past [2]. The framework is flexible enough to also allow the integration of user-supplied optimisers and accordingly different optimisers were successfully integrated and used for aerodynamic design [1,2,3].

7. Results

The validation of an optimisation process is a difficult task and the optimal solution is rarely known in advance. Therefore, in a first attempt, the thickness of the wing is free to decrease in order to check the robustness of the chain and to verify that the different strategies actually design the wing with thin profile. This is of course not a realistic design and in the last chapter a perspective for aerodynamic redesign is given and constraints on thickness are applied.

7.1. *Hybrid Mesh and Gradient Free Optimiser.*

In the first optimisation, the vertical positions of 8 lattice points are used as design variables, as depicted in Fig. 2, and a complete new hybrid mesh is generated for each new configuration. As already pointed out above, a well converged CFD solution on the hybrid mesh is rather long for optimisations involving hundred of computations. The reduction of CFD iterations shortened the CPU time but introduces inaccuracy – or noise – in the design process. The subplex approach was originally designed to optimise noisy function and is therefore here preferred [27]. However, too noisy functions slow down the design process and a compromise between number of CFD iterations and design cycle has to be found.

For the present case, the drag and lift coefficients are converged within 1 count after 1,200 CFD iterations. Using 16 CPUs of a SUN AMD Opteron, one optimisation cycle needs 49 minutes divided into 40 minutes for the RANS solver (parallel mode), 2.4 minutes for the geometry modelling (sequential mode), 6 minutes for the hybrid mesh generation (sequential mode). The design process is running for 153 design cycles (see Fig. 6) with a total turn around time slightly bigger than 5 days. When failures occur during the mesh process, an artificially high value is set to the objective function in order to reject the design and then the design process continues. It can be observed that during the design process, the TAU code is robust and efficient enough to keep the lift constant by finding the appropriate angle of incidence. (see Fig. 6).

As expected, the new wing geometry is thinner in all sections (see Fig. 7) and a new wing-fuselage intersection has been computed accordingly.

In addition a well converged computation is performed for the optimised configuration and gives a drag reduction of 9.6 drag counts (see Table 1). The drag decomposition analysis indicates that drag improvement comes mainly from the fuselage.

In fact, at a given angle of incidence, the designed wing produces more lift than the original one and to retrieve the initial lift, the angle of incidence had to be decreased by about 0.75 degrees. This confirms that the design of a wing has to be performed with the fuselage when the angle of incidence is used in the design process.

To conclude, the combination of hybrid mesh with the gradient free approach is very flexible and complex configurations can be treated without lengthy preparation. However, the design process itself is rather expensive. This restricts the use of such an approach to design problems with a limited number of design parameters.

7.2. *Mixed Mesh and Gradient Free Optimiser*

A second optimisation with the same parametrisation and optimiser has been started on the coarse mixed mesh. Following the mesh strategy described above, an identical mesh topology is ensured during the whole design process. Each computation can then be started from a previous solution and this makes the CFD process more robust in the transient phase and more efficient: a well converged solution is obtained within 3,000 cycles. One single optimisation cycle is obtained in 18 minutes using 16 CPUs and the sequential mesh process only needs 2.3 minutes. The total turn around time for a single design cycle is about 23 minutes. The design process runs for 132 cycles which represent a total turn around time of about 2.1 days (see Fig. 8).

The best solution is obtained after 107 solutions and for comparison purposes, recomputed on the finest mixed mesh. The new design has an improvement of about 27 drag counts and is almost 20 drag counts more than for the design obtained with the hybrid mesh. This is due to the fact that the mixed mesh approach shows significantly larger flow separations on the wing for the baseline configuration than observed using the hybrid mesh. Therefore a greater improvement of the wing flow is possible. This is confirmed by a larger drag reduction of the wing drag compared to the fuselage drag (see Table 1) and a smaller flow separation area on the designed wing (see Fig. 9).

This second design gives a thinner wing than the first one (see Fig. 10) and two design parameters almost reached the limit of allowed deformation: the geometry is as thin as the design process allows to it be and leads to unconventional shape at the wing tip.

The design process based on the mixed mesh is faster than for the hybrid mesh. This is due to the robustness and consistency of the mesh process. However, it can be pointed out that the design was performed on the coarse mixed mesh and the conclusion regarding the robustness can not be directly applied to the fine mixed mesh. Indeed, with the latter applied to the thin design, the mesh process failed during the deformation phase. In order to perform the comparison, the unstructured part was then completely regenerated.

To conclude, the mixed mesh process allows more efficient design but its set up is less flexibility than the hybrid one.

7.3. *Mixed Mesh and Gradient Based Optimiser*

A step forward in efficiency is now investigated by testing a gradient based optimiser. Indeed, they are well known to quickly converge but are highly sensitive to the accuracy of the gradient. Two ways of computing the gradients are investigated: the classical approach with finite differences and the adjoint approach.

One of the problems while using finite differences is the choice of an adequate finite step to get an accurate gradient. Indeed, a small step size is desired to reduce the non linearity of the design problem. On the other hand, a too small change of geometry would produce a too small change of aerodynamic drag which could be of the same order of magnitude as the numerical noise: the resulting approximated gradient would not be exact at all. Plotting the approximated gradient according to the step size

indicates a specific range lying between the two mentioned boundaries where the gradient remains almost independent of the step size. A way to improve the accuracy consists of computing the gradient with central finite differences: this approach is twice as expensive as forward finite differences but the gradient is less sensitive to the step size. In the present case, 5 different step sizes for the central finite differences were tested to find the best gradient.

In a second approach, the gradients are computed using the adjoint approach: the gradients are more efficiently and theoretically more accurately evaluated. However, the adjoint flow is computed with the assumption that the turbulent terms are frozen and this assumption introduces some inaccuracy in the gradient evaluation, as already observed on 2d cases [10]. For the baseline F6 configuration, the turbulent terms are influenced by the flow separations located on the upper wing and this may be the reason of the differences observed in the gradient computed with finite differences and with adjoint (see Fig. 11).

Regarding the efficiency, the central finite differences requires 16 CFD solutions to evaluate the gradients of 8 design variables which represent 5.4 hours turn around time if the computations are performed on 16 CPUs. In contrast, only two adjoint solutions - one for the drag and one for the lift - and the metric sensitivities are required. The current adjoint version is not running in parallel but each contribution can be evaluated simultaneously. Therefore, the simultaneous computations on three processors allow to compute the gradients in about 2 hours. It has been observed that the time required is only weakly dependant on the number of design parameters.

Using the same parameterisation and mixed mesh process as before, a first design with the conjugate gradient and central finite differences is performed. The design process is well converged after 108 CFD evaluations and 74% of the time is purely spend for the evaluation of the gradients. The turn around time is of about .1.7 days on 16 CPUs.

The second optimisation with the adjoint approach is faster and only 34 CFD evaluations are required including 5 adjoint computations and the turn around time is now of 1 day.

The convergence of both design processes is plotted in Fig. 12. For clarity purposes, only the best solutions obtained during the line search are plotted. It can be observed that both design convergence behaviours are almost identical, not only for the objective function but also for the angle of incidence. As expected, the design process with central finite differences converges a little further than with the adjoint.

The computation on the fine mixed mesh confirms the drag improvement of about 25 drag counts for both configurations, but surprisingly the design with adjoint has 2 drag counts less than the design with finite differences. It can be pointed out that the wing tip is extremely thin and small changes modify the CFD solutions.

All three designs obtained on the mixed meshes (gradient free, conjugate gradient with finite differences and with adjoint) give consistent results with almost the same geometry and the same drag improvement. A step forward in efficiency is achieved with the gradient based approach and even further with the adjoint approach. But the gain in efficiency introduces loss in flexibility: the solution has to be accurately computed, failure in the design process has to be carefully taken into account and a lengthy case dependant preparation is needed to estimate the appropriate step size for the finite differences. The adjoint approach is less sensitive to the step size, but still requires a well converged solution, both for the CFD and the adjoint solver. Furthermore a special analysis tool has to be developed to compute the gradient with the adjoint and the mesh procedure should ensure the same number of point during the design process which implies the use of a robust mesh deformation technique for unstructured meshes.

7.4. Redesign with Geometrical Constraints

In this last chapter, the thickness distribution is frozen in order to perform a more realistic redesign. The parametrisation is based on the free form deformation with the same lattice mesh, but now the displacement of one point at the upper part produce the same displacement of the corresponding point at the lower part. This ensures a constant thickness distribution during the complete optimisation. In order to broaden the design space, the lattice points at a given spanwise position can move to produce a wing twist deformation. In total 9 design parameters are used to modify the wing shape, 6 for the camberline and 3 for the twist.

A second finest parameterisation has been developed based on the previous lattice. By defining 3 more sections in spanwise and streamwise directions, one obtains a fine lattice mesh with 82 points. By using the same approach as before, the camberline and twist are then parametrised with 32 and 6 variables, respectively. Here again the wing-fuselage intersection line is recomputed each time.

Regarding the mesh process, the coarse mixed mesh is used, and optimal solutions are recomputed on the fine one.

The design process involving reduced number of design parameters is solved with the subplex approach and requires 5.2 days of turn around time to perform 323 design cycles using 16 CPUs. The second design process uses the conjugate gradient optimiser with gradients computed with the adjoint approach. After 22 design cycles including 4 gradients evaluations no better solution is found and the design process stops: the total turn around time is 18 hours using 16 CPUs.

Both designs are then recomputed on the fine mixed mesh for comparison purposes. The drag improvement on the design with only 9 parameters is rather small and is mainly due to the fuselage part thanks to a decrease of angle of incidence. On the other hand, the design with 42

design parameters gives an improvement of about 18 drag counts with a significant contribution from the wing part (see Table 1).

The pressure distribution at the upper surface of the wing for the baseline and optimised geometries are given in Fig. 13. It can clearly be observed that the suction peak and the strong shock are only reduced on the design with larger design parameters.

8. Summary and Conclusion

An aerodynamic shape optimisation environment based on the unstructured RANS solver *TAU* code has been developed. This aerodynamic chain is based on advanced strategies like among others the free form geometry deformation, the hybrid and mixed structured/unstructured mesh processes and the adjoint approach. This chain is applied successfully for the wing design of the DLR-F6 configuration where the wing-body intersection line is updated during the design process. This application permits to classify different strategies towards their capabilities to be reused for other design problems (flexibility) and the time required to solve the problem (efficiency). The hybrid mesh approach coupled with a gradient free approach is the most flexible strategy tested but shows the longest turn around time. In contrast, the mixed mesh process together with the adjoint approach is the most efficient and permits to solve design problems of greater dimension at lower cost. However, a drastic loss in flexibility has been observed due to the mesh process and the adjoint approach itself.

Some weakness in the developed design process has been identified and mainly concerns the robustness of the mesh deformation approach, the adjoint solver and its corresponding way to compute the gradient. After an improvement of the present design process, near future activities will focus on more complex configurations, like the engine integration. In a second step, multi-points will be addressed. A step closer to real aircraft design will be achieved by first introducing the wing structural effects and finally by resolving the corresponding multi-disciplinary optimisations.

9. References

[1] Brezillon, J., Dwight, R., "Discrete Adjoint of the Navier-Stokes Equations for Aerodynamic Shape Optimisation", EUROGEN 2005, Munich, September 2005.

[2] Brezillon, J., Gauger, N.R., "2D and 3D aerodynamic shape optimization using the adjoint approach", Aerospace Science and Technology, Vol. 8, No. 8, 2004, pp. 715-727.

[3] Brezillon, J., Wild, J., "Evaluation of different optimization strategies for the design of a high-lift flap device", EUROGEN 2005, Munich, 2005.

[4] Brodersen, O., Hepperle, M., Ronzheimer, A., Rossow, C.-C., Schöning, B., "The Parametric Grid Generation System MegaCads", Numerical grid generation in computational field simulations; Proceedings of the 5th International Conference, edited by B.K. Soni, Mississippi State Univ, 1996. pp. 353-362.

[5] Brodersen, O., Rakowitz, M., Amant, S., Larrieu, P., Destarac, D., Sutcliffe, M., "Airbus, ONERA, and DLR Results from the Second AIAA Drag Prediction Workshop", AIAA Journal of Aircraft, Vol. 42, No. 4, 2005, pp. 932-940.

[6] Brodersen, O., "Drag Prediction of Engine-Airframe Interference Effects Using Unstructured Navier-Stokes Calculations", AIAA Journal of Aircraft, Vol. 39, No. 6, 2002, pp. 927-935.

[7] CentaurSoft: URL http://www.centaursoft.com, 2006.

[8] 3rd Drag Prediction Workshop, AIAA: URL: http://aaac.larc.nasa.gov/tsab/cfdlarc/aiaa-dpw , 2006

[9] Dwight, R., "Efficiency Improvements of RANS-Based Analysis and Optimization using Implicit and Adjoint Methods on Unstructured Grids", School of Mathematics, University of Manchester, 2006.

[10] Dwight, R., Brezillon, J., "Effect of Various Approximations of the Discrete Adjoint on Gradient-Based Optimization", Proceedings of the 44th AIAA Aerospace Sciences Meeting and Exhibit, AIAA Paper 2006-0690, Reno NV., Jan. 2006.

[11] Dwight, R., Brezillon, J., Vollmer, D., "Efficient Algorithms for Solution of the Adjoint Compressible Navier-Stokes Equations with Applications", Proceedings of the ONERA-DLR Aerospace Symposium (ODAS), Toulouse, 2006

[12] Edwards, J., Chandra, S., "Comparison of Eddy Viscosity-Transport Turbulence Models for Three-Dimensional Shock-Separated Flowfields", AIAA Journal of Aircrafts, Vol. 34, No. 4, 1996, pp. 756-763.

[13] Frommann, O., "SynapsPointerPro V2.50", Synaps Ingenieur-Gesellschaft mbH, Bremen, 2002

[14] Gerhold, T., and Evans, J., "Efficient Computation of 3D-Flows for Complex Configurations with the DLR-TAU Code Using Automatic Adaptation", Notes on Numerical Fluid Mechanics, edited by W. Nitsche, H.-J. Heinemann, and R. Hilbig, Vol. 72, Vieweg, Braunschweig, 1998, pp. 178-185.

[15] Gerhold, T., "Overview of the Hybrid RANS Code TAU", Notes on Numerical Fluid Mechanics and Multidisciplinary Design, edited by N. Kroll and J. Fassbender, Vol. 89, Springer, Berlin, 2005, pp. 81-92.

[16] Jameson, A., Martinelli, L., Pierce, N.A., "Optimum Aerodynamic Design using the Navier-Stokes Equations", Theoret. Comput. Fluid Dynamics, Vol. 10, Springer, 1998, pp. 213-237.

[17] Kallinderis. Y., "Hybrid Grids and Their Applications", Handbook of Grid Generation, edited by J.F. Thompson, B.K. Soni, and N. Weatherill, CRC Press, Boca Raton, FL, 1999, pp. 25.1-25.18.

[18] Kroll, N., Gauger, N. R., Brezillon, J., Becker K., Schulz V., "Ongoing Activities in Shape Optimization within the German Project MEGADESIGN", ECCOMAS 2004, Jyväskylä, Finland, 24-28 July 2004.

[19] Kroll, N., Rossow, C.-C., Becker, K., Thiele, F., "MEGAFLOW – A Numerical Flow Simulation System", 21st ICAS Symposium, Paper 98-2.7.4, Melbourne, Australia, 1998.

[20] Kroll, N., Rossow, C.C., Becker, K., Thiele, F., "The MEGAFLOW project", Aerospace Science and Technology., Vol. 4, 2000, pp. 223-237.

[21] Kroll, N., Rossow, C.-C., Schwamborn, D., Becker K., Heller, G., "MEGAFLOW - A Numerical Flow Simulation

Tool for Transport Aircraft Design", Paper 1.10.5, ICAS 2002 Congress, 2002.
[22] Laflin, K.R., Klausmeyer, S.M., Zickuhr, T., Vassberg, J.C., Wahls, R.A., Morrison, J.H., Brodersen, O.P., Rakowitz, M.E., Tinoco, E.N., Godard, J.L., "Data Summary from the Second AIAA Computational Fluid Dynamics Drag Prediction Workshop", AIAA Journal of Aircraft, Vol. 42, No. 5, 2005, pp. 1165-1178.
[23] Mavriplis, D,J, "A Discrete Adjoint Approach for Optimization Problems on Three-Dimensional Unstructured Meshes", Proceedings of the 44th AIAA Aerospace Sciences Meeting and Exhibit, AIAA Paper 2006-50, Reno NV., Jan. 2006.
[24] Nelder, J.A., Mead, R., "A Simplex Method for Function Minimization", Computer Journal, Vol. 7, 1965, pp. 308-313.
[25] Ronzheimer, A., "Shape Based On Freeform Deformation In Aerodynamic Design Optimization", ERCOFTAC Design Optimization International Conference, March 31.-April 2. 2004 Athens, Greece.
[26] Ronzheimer, A., "Shape Parameterization in Multidisciplinary Design Optimisation Based on Freeform Deformation", EUROGEN 2005, Munich, Sept. 2005
[27] Rowan, T., "Functional Stability Analysis of Numerical Algorithms", Thesis, Department of Computer Sciences, University of Texas at Austin, USA 1990.
[28] Schöberl, J., "NETGEN - An advancing front 2D/3D mesh generator based on abstract rules", Computing and Visualization in Science, Vol. 1, 1997, pp. 41-52.
[29] Spalart, P.R., and Allamaras, S.R., "A One-Equation Turbulence Model for Aerodynamic Flows", AIAA Paper 92-0439, Jan. 1992.
[30] Vanderplaats, G.N., "Numerical Optimization Techniques for Engineering Design", McGraw-Hill Series in Mechanical Engineering, ISBN 0-07-066964-3, 1984
[31] Wild, J., "Validation of Numerical Optimization of High-Lift Multi-Element Airfoils based on Navier-Stokes-Equations", AIAA Paper 2002-2939, June 2002.
[32] Wild, J., "Multi Objective Constrained Optimization and High Lift Device Applications", Van Karman Institute, VKI Lecture Series 2004-07, ISBN 2-930389-56-7, Brussels, 2004.
[33] Wild, J., "Acceleration of Aerodynamic Optimization Based on RANS-Equations by Using Semi-Structured Grids", Proc. ERCOFTAC Design Optimization: Methods & Applications, Athens (Greece), Paper ERCODO2004_221, 2004
[34] Wild, J., Niederdrenk, P., Gerhold, T., "Marching Generation of Smooth Structured And Hybrid Meshes Based on Metric Identity", Proceedings of the 14th International Meshing Roundtable, edited by B. Hanks, Springer, Berlin, 2005, pp. 109-127.
[35] MPI: Message Passing Interface, URL: http://www-unix.mcs.anl.gov/mpi , 2006

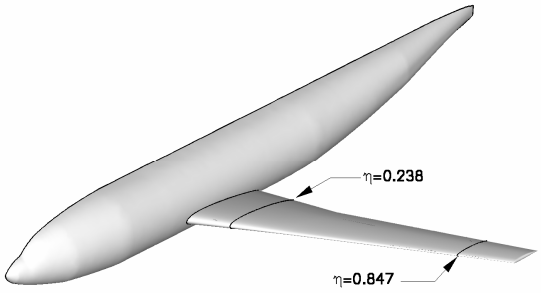

Fig. 1. Illustration of the DLR F6 wing-body configuration.

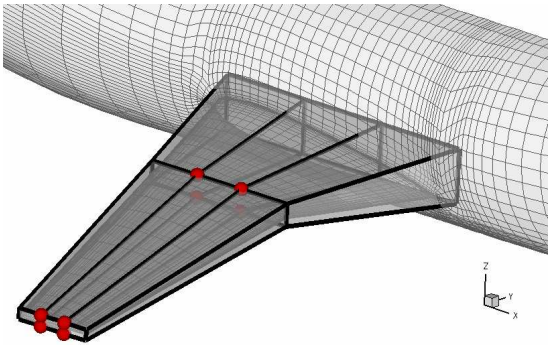

Fig. 2. Lattice grid of the free form deformation and design parameter (sphere).

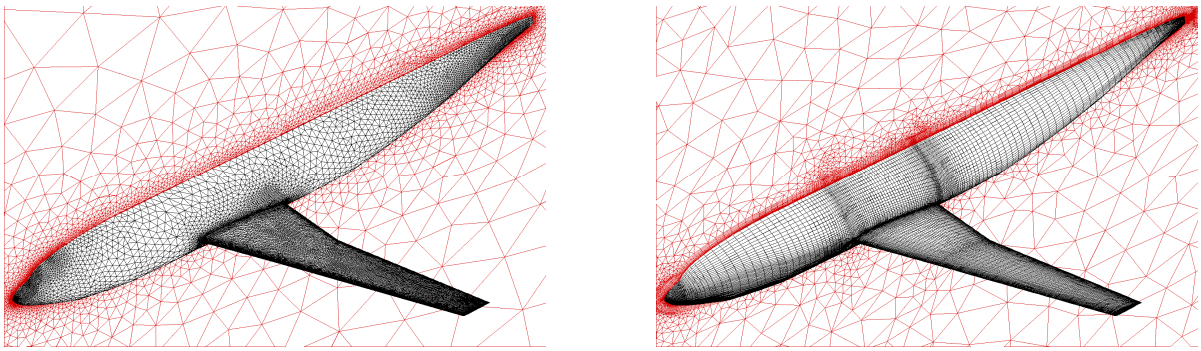

Fig. 3. Navier-Stokes meshes of the DLR-F6 configuration
(Hybrid mesh on the left – Mixed structured/unstructured mesh on the right).

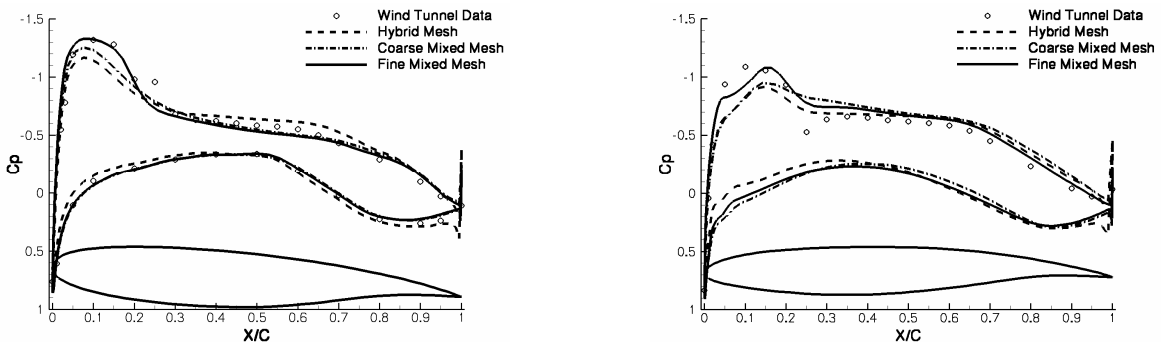

Fig. 4. Geometry and pressure distribution at 2 sections (η =0.238 on the left and η =0.847 on the right).

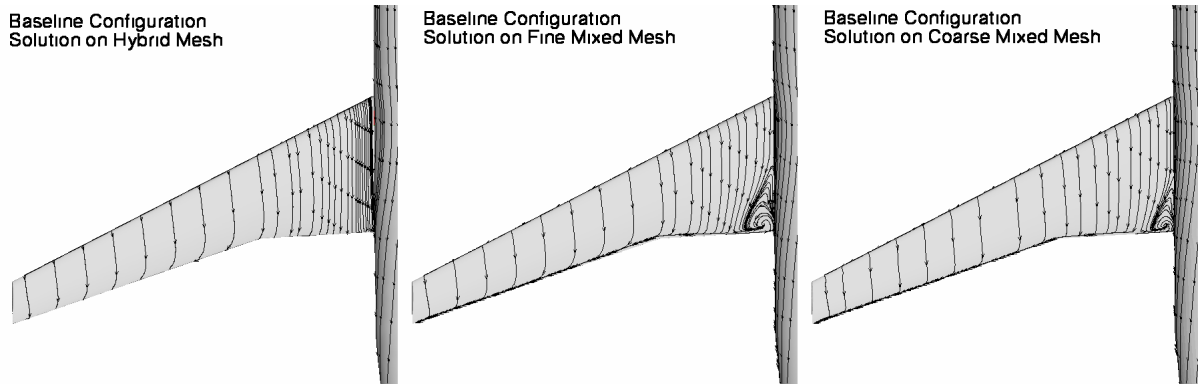

Fig. 5. Streamtraces on the upper wing for the baseline configuration.

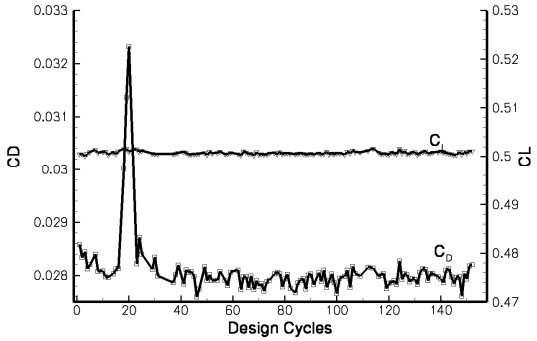

Fig. 6. Convergence of the design process (8 design parameters, hybrid mesh and Subplex).

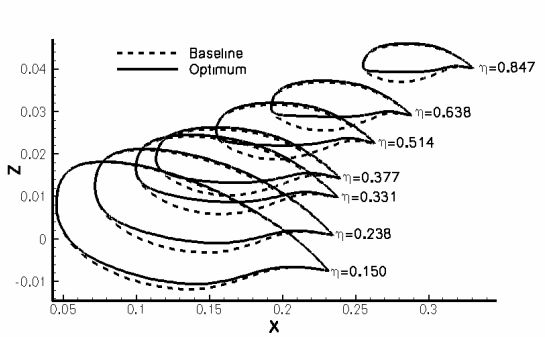

Fig. 7. Geometry slices of the baseline and optimised wing (8 design parameters, hybrid mesh and Subplex).

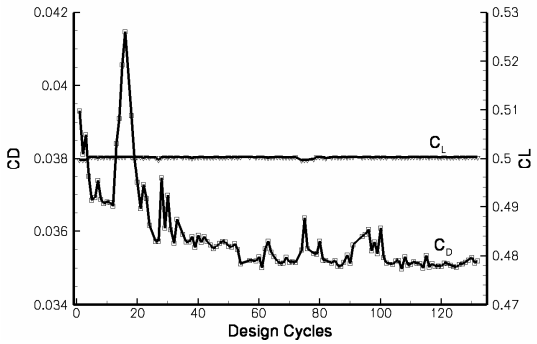

Fig. 8. Convergence of the design process (8 design parameters, mixed mesh and Subplex).

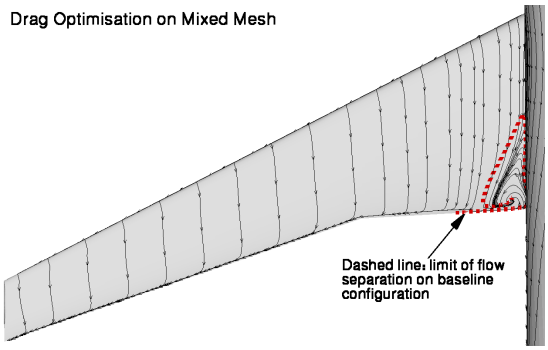

Fig. 9. Streamtraces obtained on fine mixed mesh Optimised geometry with Subplex and mixed mesh.

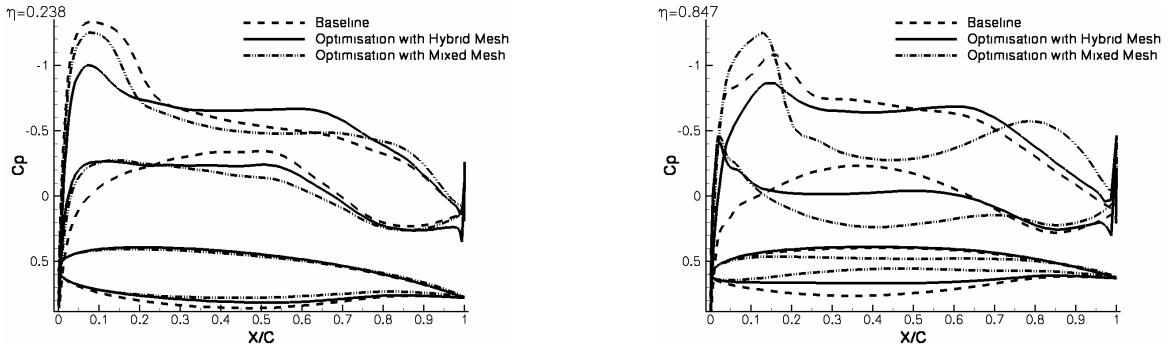

Fig. 10. Geometry and pressure distribution at sections η =0.238 and η =0.847 (Optimisation with Subplex – 8 design parameters).

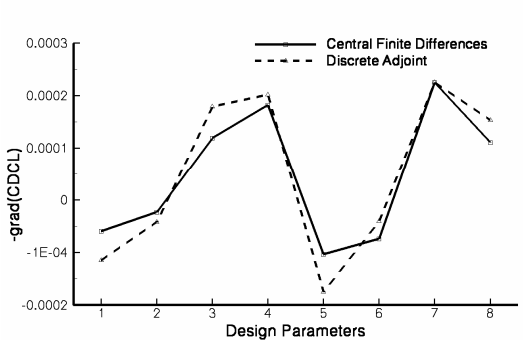

Fig. 11. Gradient of the objective function (8 design parameters, coarse mixed mesh).

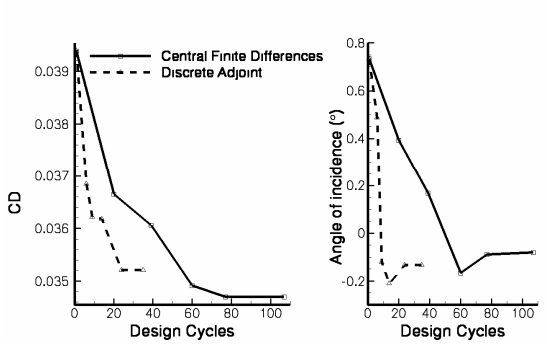

Fig. 12. Convergence with Conjugate Gradient opt. (8 design parameters, mixed mesh).

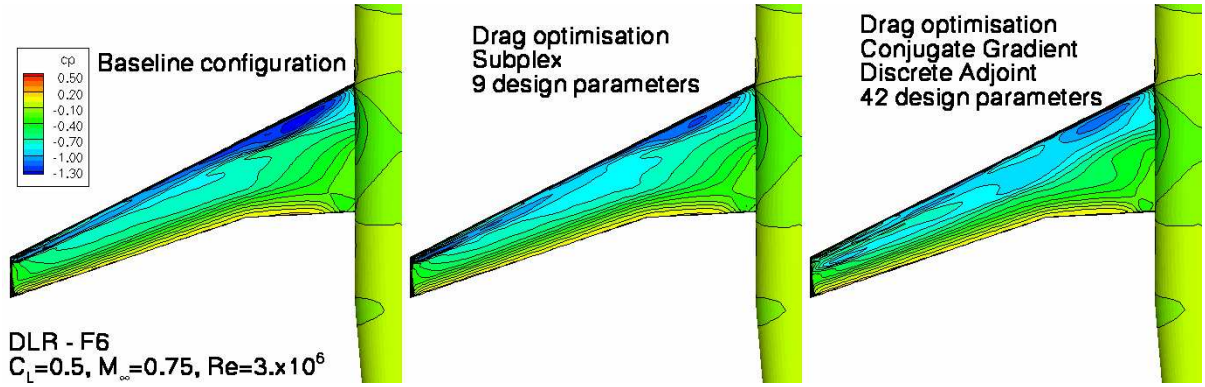

Fig. 13. Surface pressure coefficient contours on initial DLR-F6 configuration Optimisation with 9 design parameters and with 42 design parameters.

Strategy	Δα(°)	C_L	ΔC_D x10^{-4} Total	ΔC_D x10^{-4} Wing	ΔC_D x10^{-4} Fuselage
Hybrid mesh+SubPlex	-0.75	0.500	-9.6	+0.1	-9.7
Mixed mesh+SubPlex	-0.97	0.500	-27.2	-19.8	-7.5
Mixed mesh+Gradient	-0.87	0.500	-24.1	-17.8	-6.3
Mixed mesh+Adjoint	-0.94	0.500	-25.9	-18.3	-7.6
Design with 9 param.	-0.30	0.500	-1.4	+1.2	-2.6
Design with 42 param.	-0.29	0.500	-17.7	-16.1	-1.6

Table 1. Drag improvement for the different designs.